Practical approaches to assess thermal performance of a finned heat sink prototype for low concentration photovoltaics (LCPV) systems

González Gallero, Francisco Javier; Rodríguez Maestre, Ismael; Hemida, Hassan; Álvarez Gómez, Pascual

DOI:
10.1016/j.applthermaleng.2019.04.086

Document Version
Peer reviewed version

Citation for published version (Harvard):
González Gallero, FJ, Rodríguez Maestre, I, Hemida, H & Álvarez Gómez, P 2019, 'Practical approaches to assess thermal performance of a finned heat sink prototype for low concentration photovoltaics (LCPV) systems: analytical correlations vs CFD modelling', *Applied Thermal Engineering*, vol. 156, pp. 220-229. https://doi.org/10.1016/j.applthermaleng.2019.04.086

Practical approaches to assess thermal performance of a finned heat sink prototype for low concentration photovoltaics (LCPV) systems: Analytical correlations vs CFD modelling

Francisco Javier González Gallero[1]*, Ismael Rodríguez Maestre[1], Hassan Hemida[2], Pascual Álvarez Gómez[1]

[1]Escuela Politécnica Superior de Algeciras. University of Cadiz. Spain.
[2]School of Engineering. University of Birmingham. United Kingdom.

*Corresponding author. Tel.: +34 956 028000. E-mail address: javier.gallero@uca.es
Postal address:
Escuela Politécnica Superior de Algeciras
Avenida Ramón Puyol s/n
11202 Algeciras
Spain

Abstract

The performance of a low-cost extruded heat sink prototype for a Low Concentration Photovoltaics system is studied using various analytical correlations and CFD simulations. An experimental test, with temperature measurements at different monitoring points of heat sink surface, was carried out in order to select the most appropriate approach. Large deviations (of up to 20°C) in the estimation of base plate temperature from correlations were found when compared to experimental results, probably due to the specific geometry characteristics of the heat sink, with variable fin thickness and high fin length. Furthermore, discrepancies of up to 48% have been found among the different correlations. The numerical CFD results of temperature at monitoring points and at the base plate showed relative errors of about 1%, which were at least 15 times smaller than the results given by analytical correlations. Also, numerical simulations allowed the identification of stagnation zones due to the great length of the heat sink and characteristic air flow patterns, which help to explain its performance under different operating conditions. Thus, results showed that multiple chimney flow pattern and air stagnation zones seem to disappear for inclination angles greater than 30°.

Keywords
Low concentration photovoltaics, heat sink, analytical correlations, numerical simulations.

Nomenclature			
A	Convective area (m^2)	T_b	Temperature at base plate (°C)
B	Base plate thickness (m)	T_0	Temperature at reference point (°C)
C	Dimensionless constant	t_e	Equivalent and constant fin thickness (m)
Gr	Grashof Number, $\boldsymbol{Gr} = \frac{g\beta L_C^3(T-T_a)}{\nu^2}$	t_p	Fin thickness at tip of fin (m)
Gr'	Modified Grashof Number	t_p'	Fin thickness at tip of fin (m) (fins at the extreme ends of heat sink)
g	Gravitational acceleration (ms^{-2})	V	Characteristic velocity (ms^{-1})
h	Convective heat transfer coefficient ($W/(m^2K)$);	W	Heat sink width (m)
k	Air thermal conductivity ($Wm^{-1}K^{-1}$)	y+	Dimensionless distance to the wall
L	Heat sink length (m)	*Greek symbols*	

L_C	Characteristic length (m)	α	Thermal diffusivity (m^2s^{-1})
m	Dimensionless exponent	β	Thermal expansion coefficient (K^{-1})
N	Number of fins	ε	Emissivity
n	Dimensionless exponent	ν	Kinematic viscosity (m^2s^{-1})
Nu	Nusselt Number, $\boldsymbol{Nu} = \frac{\boldsymbol{hL_C}}{\boldsymbol{k}}$	ρ	Density (kgm^{-3})
Q	Heat flux (W)	ρ_0	Density at reference point (kgm^{-3})
Ra	Rayleigh Number, $\boldsymbol{Ra} = \boldsymbol{Gr} \cdot \boldsymbol{Pr} = \frac{\boldsymbol{g\beta L_C^3(T-T_a)}}{\boldsymbol{\alpha\nu}}$	θ	Inclination angle with respect to horizontal (°)
Re	Reynolds Number, $\boldsymbol{Re} = \frac{\boldsymbol{VL_C}}{\boldsymbol{\nu}}$	*Subscripts*	
S	Fin spacing (m)	a	Ambient air
S_e	Equivalent and constant fin spacing (m)	b	Base plate
t	Fin thickness (m)	e	equivalent
T	Temperature (°C)	i	index
t_b	Fin thickness at the base (m)	p	Tip of the fin
t_b'	Fin thickness at the base (m) (fins at the extreme ends of heat sink)	0	Reference point
T_a	Ambient temperature (°C)		

1.- Introduction

Solar Photovoltaic (PV) systems have been developing very fast during the last years and are playing an important role in the production of electricity from solar energy worldwide [1]. In Concentration Photovoltaics (CPV), which is a combination of optical and PV technology, a large area (aperture) of sunlight is focused on a smaller area solar cell, by using optical collectors such as lenses or mirrors. Consequently, cost reduction through the use of less PV material allows the use of more expensive and high-efficiency cells. Significant development in CPV research and technology has been achieved recently, reporting solar cell efficiencies up to 46% [2] which is notably higher than the efficiency of standard PV systems (between 6% and 25% under optimal operating conditions).

CPV systems can be classified depending on their optical or flux concentration ratio, defined as the energy flux ratio at the aperture and at the receiver. Systems with concentration ratios from 2 to 30 are called Low Concentration Photovoltaics (LCPV) systems, and those with a concentration ratio higher than 100, High Concentration Photovoltaics (HCPV) systems.

The most important parts of CPV are the optical concentrator, the heat sink and the sun-tracker [3]. Tracking is required to achieve high cell performance and, although it is a complex electro-mechanical part of the system, it allows producing a larger amount of electrical energy during the day. The increase of concentration in HCPV systems demands a precise optics and tracking system in order to capture direct radiation [4]. In contrast, LCPV systems usually require single-axis tracking, their sensitivity to tracking errors is smaller and can capture a larger fraction of diffused radiation than HCPV systems [5].

It is well-known that efficiency of solar PV cells decreases with an increase in temperature [6]. Thus, a proper cooling of the operating surface of PV systems can improve the electrical efficiency and also decrease the rate of degradation with time [7]. Natural convection is the most critical heat

transfer process in passive heat sinks. Given the narrow range of heat transfer coefficients available for natural convection or buoyancy driven air cooling (between 1 and 10 W/m^2K) [8], the most effective way of lowering the fluid-side thermal resistance is by increasing the area of the 'wetted' surface. This is achieved by using fins. Finned heat sinks are widely used in different fields and some authors [9] have shown they are more effective than flat back plates in LCPV devices. It has also been observed that radiation, which is highly dependent on heat sink surface emissivity, can contribute around 20% of the total heat dissipation [10]. Rammohan Rao and Venkateshan [11] made an interferometric study in which they highlighted the importance of mutual interaction between free convection and radiation.

This work is focused on a low-cost extruded finned heat sink, designed as a prototype to cool a LCPV system (Fig.1). It is made from aluminium with a low surface emissivity and it has variable thickness fins with an unusually high length (1m approximately).

In addition to experimental tests, there are different practical approaches that can be found in the scientific literature in order to address thermal performance of a heat sink under natural convection: correlations that usually provide the overall (convective or combined convective-radiative) heat transfer coefficient, and numerical models, such as those based on Computational Fluid Dynamics (CFD), which are also able to estimate temperature distribution along the heat sink and air temperature and velocity fields.

A high number of theoretical, numerical and experimental investigations, from which correlations are mainly derived, have been developed on heat transfer from fins on a horizontal surface, the majority of them on rectangular fin arrays because they are simple and easy to manufacture. From heat transfer rate and the overall heat transfer coefficient given by correlations, temperature difference between the heat sink and the air can be estimated using the Newton's law of cooling. The selection of an appropriate correlation is an important issue since significant discrepancies in the estimation of Nusselt number (dimensionless ratio of convective to conductive heat transfer) have been reported by some authors (relative errors of 50% [12] and 25% [13]).

There are several points that must be considered and can limit the application of the different correlations, such as geometric similarity, the inclusion (or not) of radiation heat transfer and also air flow regime. Thus, correlation from Tari and Mehrtash [14] was obtained for height to length fin ratios between 0.015 and 0.10, while that from Jones and Smith [13] was given for a wider range of the same ratio (between 0.026 to 0.19). Most correlations estimate an overall convective heat transfer coefficient ([12], [15], [16], [17], [18], [19], [20]), and only a few include the combined effect, allowing the estimation of an overall convective-radiative coefficient [10]. In relation to air flow conditions, there are correlations for which values of Rayleigh number (Ra) are also limited. Thus, the lower limit of Ra for the correlation provided by Rao et al. is 2300 [10], while it is 200 for Jones and Smith's correlation [13]. Therefore, despite their apparent diversity, a study of the correlations that could be suitable to the present heat sink is necessary.

Conversely, different numerical models based on CFD ([21], [22], [23], [24], [25], [26]) have been applied to a variety of heat sink configurations under natural convection with different purposes: obtain the optimum fin spacing and shape, study the air flow around the heat sink to investigate the relevant factors affecting its performance, analyse new designs of heat sinks, etc. A summary of these studies and main issues is given in Table 1. Conjugate heat transfer (CHT) is usually used, which models the heat transfer between a solid object and a fluid flowing over it. Air flow is generally treated as 3D steady laminar flow. In most cases, numerical results are compared with experimental measurements, usually in terms of heat transfer coefficient, surface base temperature or thermal resistance, providing relative errors between 5 and 10%. Numerical simulations allow not only the estimation of temperature fields and heat fluxes but also the study of flow patterns, such as the characteristic single and double chimney patterns of rectangular fin

arrays, which were confirmed first by Harahap and McManus [27] from experimental observations. In view of their potential, CFD techniques can be an interesting alternative to correlations for this kind of heat sinks.

CFD study	Heat sink configuration	2D / 3D	Steady/ transient	Laminar/ Turbulent	Air density, ρ	Radiation model	Software program	Experimental validation	Maximum Error (%)	Objectives	Main conclusions
Dogan et al. (2014) [21]	Rectangular	3D	Steady	Laminar	$\rho=\rho(T)$	Surface to surface (S2S)	Ansys Fluent v12.1	Yes, (Harahap & McManus experimental data)	5.5% (heat transfer coefficient)	Fin shape optimization (set of 6 different fin shapes)	CFD able to find optimum fin shape
Meng et al. (2018) [22]	Rectangular	3D	Steady	Laminar[1]	Boussinesq model	Not considered	Not reported	Yes (Meng et al. 2014)	10.5% (surface temperatures)	Influence of heat sink mounting angle on heat dissipation	New fin geometries to improve heat sink performance
Feng et al. (2018) [23]	Rectangular	3D	Steady	Laminar	$\rho=\rho(T)$	Discrete Ordinates (DO)	Ansys Fluent v14.5	Yes (Feng et al. 2018)	Around 5% (surface temperatures)[2]	Analyse heat performance of a novel cross-fin heat sink	New heat sink improves heat transfer compared to a reference plate-fin heat sink
Mousavi et al. (2018) [24]	Continous/ interrupted finned heat sink	3D	Steady	Laminar	Boussinesq model	Surface to surface (S2S)	Ansys Fluent	Yes (continuous finned heat sink)	Not reported	Investigate thermal performance of different vertical finned heat sinks	A decrease smaller than 3 mm in fin spacing does not improve cooling. Capped fins enhance cooling.
Costa and Lopes (2014) [25]	Radial	3D	Steady	Laminar	Boussinesq model	Monte Carlo (S2S)	Ansys CFX	No	---	Find a methodology to improve geometry configuration of a heat sink used to cool a new LED lamp	The new configuration achieves the requested target.
Effendi and Kim (2017) [26]	Hybrid (pins, finned, hollows)	3D	Steady	Laminar	Boussinesq model	Discrete Ordinates (DO)	Ansys Fluent	Yes (Effendi and Kim 2017)	10% (thermal resistances)	Investigation of orientation effects on different heat sink configurations	Smaller thermal resistance at an orientation angle of 45°. Some configurations are less dependent on orientation.

Table 1. Summary of different CFD studies on heat sink thermal performance under natural convection. [1]Low Reynolds number k-ε turbulent model is adopted. [2]Extracted from graph digitalisation.

Literature review reveals a wide diversity of methodologies that can be applied to heat sinks (due to different geometric similarity, convective-radiative effect, air flow regime, etc.) which, together with the special features of the LCPV heat sink, show the interest in developing a study to select the most suitable method. This is the main aim of the present work, that is, a review of the existing and more widespread approaches and the selection of an appropriate one to analyse thermal performance of the heat sink under study.

First, a selection of the most suitable correlations for this kind of device has been carried out. In order to assess the behaviour of correlations and CFD method, an experimental test that tried to reproduce unfavourable (free convection) operating conditions of the system was developed. Results from correlations and CFD simulations were then discussed. Finally, and after validated, the numerical model was used to predict heat sink performance under different normal operating conditions and results were compared with those from former studies.

2.- LCPV heat sink and experimental test

The device considered in this study is an extruded heat sink for LCPV, manufactured from aluminium with 13 fins of variable thickness (Fig. 1). Table 2 shows the main geometric dimensions of the heat sink. From considerations of manufacturability and strength, the ranges of fin parameters in most plate fin heat sinks produced with extrusion aluminium alloys are generally the following: fin thickness is between 1mm to 3mm; fin spacing between 1mm to 15mm; and fin height between 25mm to 50mm [28]. Due to the geometry configuration of the LCPV system (Fig. 2), the heat sink studied here has a high fin length (0.900 m).
The emissivity of the material (provided by manufacturer) is 0.09, a typical value of extruded Aluminium.

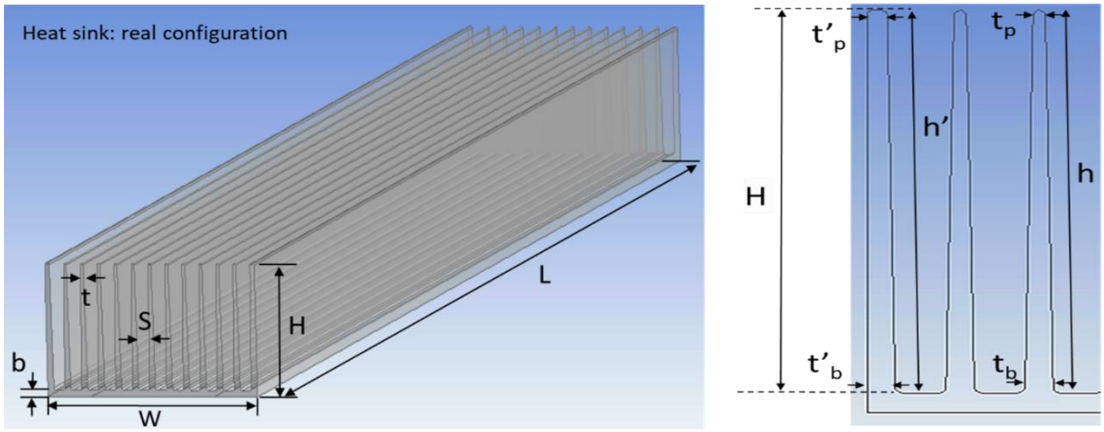

Fig. 1. Isometric view of the heat sink and main geometric dimensions (left) and fins cross section (right). Fin geometry and spacing at the base and tip are different. Fins at the extreme ends are different from the rest.

Description	Name	Value
Fin length	L (m)	0.900
Fin height	H (m)	0.060
Heat sink width	W (m)	0.120
Fin spacing	S (m)	0.0062-0.0082
Fin thickness	t (m)	0.0015-0.0035
	t'(m)[1]	0.0025-0.0035
Base plate thickness	b (m)	0.003
Number of fins	N	13
Convective area	A(m^2)	1.521
H/L	---	0.067
S/H	---	0.103-0.137
S/L	---	0.0069-0.0091

Table 2. Geometric dimensions of heat sink. [1] Fin thickness of the two fins at the extreme ends of the heat sink.

The LCPV cells are attached to the bottom surface of the heat sink, receiving sunlight from parabolic mirrors located below (Fig. 2). Thus, heat is generated along the longitudinal axis of the base plate. Cell is bond to the rear side of the heat sink by using a thermal paste of high conductivity.

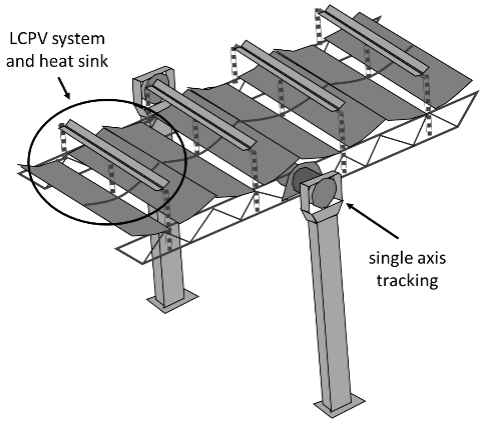

Fig. 2. Schematic of the LCPV receiver and tracking system showing the location of the heat sink.

The heat sink was subjected to an experimental test in a laboratory room without windows and carefully sealed in order to ensure conditions of natural convection. Fig. 3 shows an image of the heat sink and the data acquisition unit. The heat sink was placed with an inclination of 0° with respect to the horizontal surface. Heat source was generated by setting an electrical resistance along a strip of the bottom surface of the base plate. The remaining area of the bottom surface was thermally isolated using polystyrene (thermal conductivity of 0.03 $Wm^{-1}K^{-1}$). Electric power (calculated from voltage times electric current) was equal to 450W, simulating the real LCPV heat input (Fig. 4). Neglecting other heat losses, that value will be equal to the total heat flux (Q) by convection and radiation from heat sink.

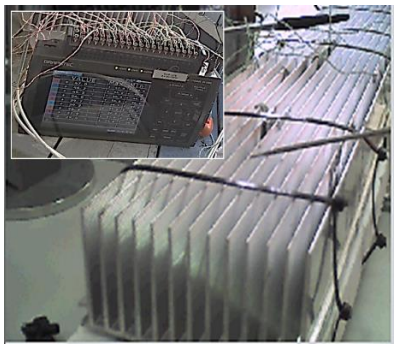

Fig. 3. Heat sink and data acquisition unit used in experimental test.

Seven K-type thermocouples, with a standard error of ±0.5°C, were located in the centre part of the heat sink to avoid edge effects. Temperature measurements were taken every second for approximately 90 minutes. Steady state conditions were considered when temperature changes at the base plate were smaller than 0.5°C during the last 5 minutes of the experiment. Final temperature values at monitoring points are shown in Table 3. Room temperature was 26.0 °C, approximately. Mean base plate temperature, calculated as the average of temperature values at points 1, 4 and 6, was about 129°C. As expected, the highest temperature was measured at point 1, while edge points 5 and 7 showed the lowest values (Fig. 5).

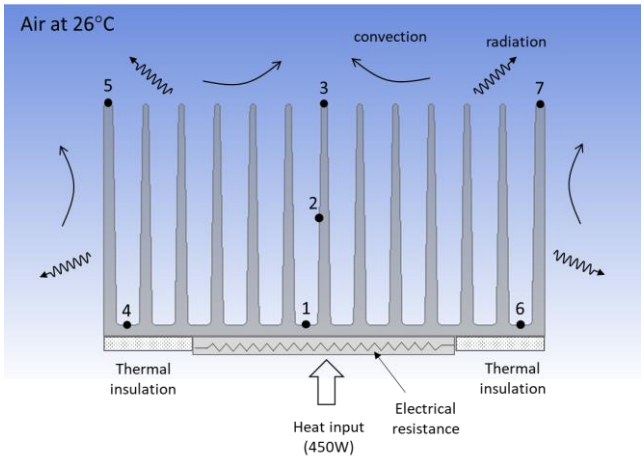

Fig. 4. Description of experimental test. Location of monitoring points (1-7, cross section at the centre of the heat sink).

T_1(°C)	T_2(°C)	T_3(°C)	T_4(°C)	T_5(°C)	T_6(°C)	T_7(°C)	T_b(°C)[1]
132.4	129.6	128.2	125.6	123.1	128.5	125.2	128.8

Table 3. Measured temperatures at monitoring points (steady state). [1]Base plate temperature calculated as the average of temperature values at monitoring points 1, 4 and 6.

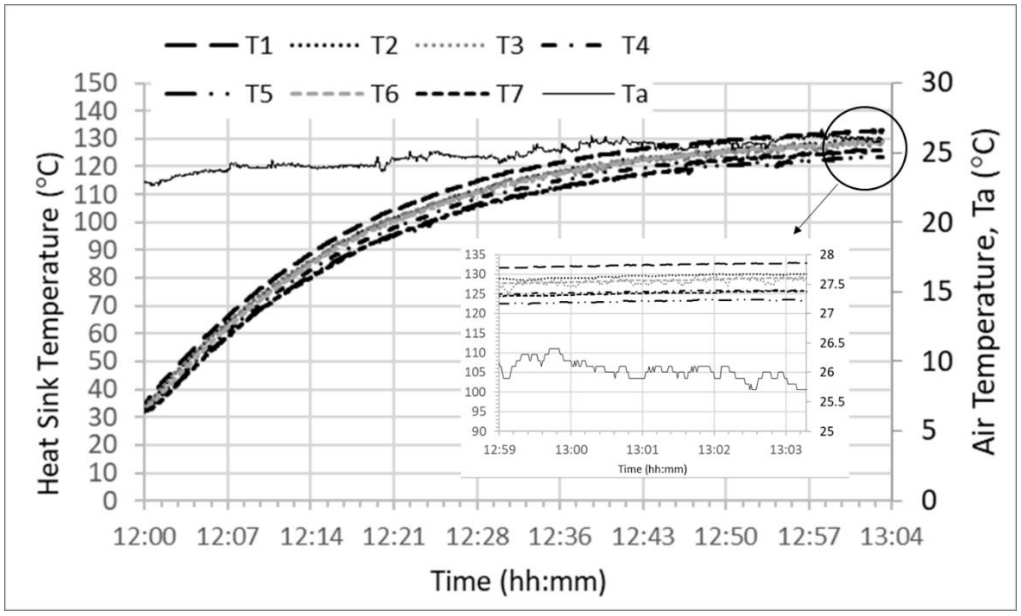

Fig. 5. Time evolution of temperature at different monitoring points on heat sink surface and room air temperature during the experimental test. Graph inside shows temperatures during the last minutes of the experiment.

3.- Correlations and estimation of heat sink base temperature

In this section, the most commonly used and applicable correlations to this kind of heat sinks have been reviewed and selected.

Although there are some studies that propose correlations for new designs of heat sinks in which the effect of tip-to-base spacing ratio is considered [29], only ratios equal or smaller than one, for which convection is enhanced, are considered. This is not the case for the heat sink under consideration for which the former ratio is greater than one. Thus, correlations suitable for horizontal base plate with vertically oriented rectangular fins of constant thickness were considered (Fig. 6). They generally provide an equation (equation (1)) for Nusselt number (Nu) in terms of standard or modified Rayleigh (Ra) number and a characteristic length, which in this case is fin spacing (S).

$$Nu = C\ Ra^n \tag{1}$$

Ra depends on the difference between the temperature at heat sink base (T_b) and ambient temperature (T_a).

When using correlations for convective heat transfer coefficient, heat flux from radiation should be calculated and subtracted from total heat flux (Q). In the present work, the radiation heat transfer, which depends on emissivity, temperature and view factors, was calculated using the simplified method suggested by Shabany [30]. This method avoids the use of complex equations for the estimation of view factors. Furthermore, errors for normalised values of L/S and H/S greater than 5, as for the heat sink the present study is focused on, are smaller than 5%. Very similar results were also obtained when using the methodology proposed by Rea and West [31].

Both Nu and radiative heat flux depend on base temperature (T_b), such that an iterative process is required. In this work, the resulting system of non-linear equations was solved using Newton-Raphson method. The error limit for T_b differences was set to 0.1°C. All air properties were estimated at film temperature (average of T_b and T_a), except thermal expansion coefficient, calculated as $1/T_b$.

As the original heat sink is not exactly an array of rectangular fins with constant thickness and spacing, equivalent dimensions were estimated. Considering that (natural) convection is the prevailing heat transfer mechanism, the condition applied here was that the equivalent heat sink (with rectangular fins of fixed thickness) had the same 'wetted' surface area as the real heat sink (Fig. 6). However, for the same exposed area, there are several geometric solutions of rectangular fins that would lead to different air flow patterns and radiative losses and, consequently, to different thermal performance. With the approach presented here, two relevant factors have been taken into account: firstly, the wetted or available surface for convective heat transfer, such that the equivalent area was set equal to the real one (what did not set the value of the equivalent fin spacing); and secondly, a characteristic air flow length scale, in such a way that the value of fin spacing at the fin base was selected as the equivalent fin spacing.

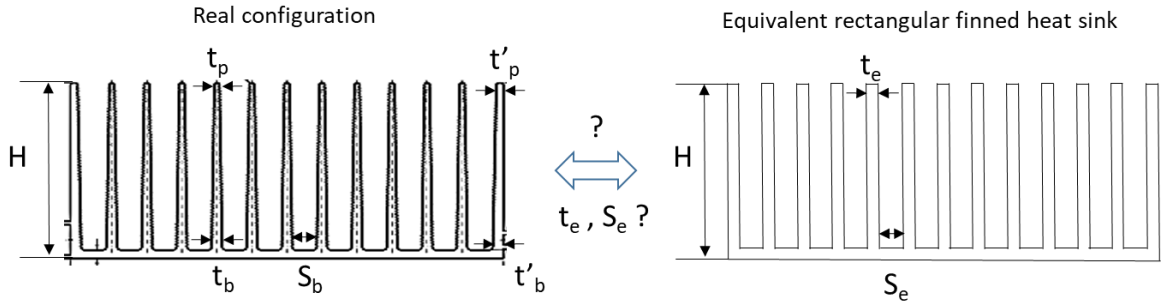

Fig. 6. Equivalent rectangular finned heat sink and geometric dimensions.

Thus, taking the equivalent fin spacing (S_e) equal to fin spacing at the base of fins (S_b) in the real configuration, the equivalent fin thickness was calculated from equation (2).

$$t_e = \frac{2t'_p L + 2H\left(t'_p + t'_b\right) + (N-2)\left(Lt_p + Ht_p + Ht_b\right)}{N(L+2H)} \quad (2)$$

From the dimensions of the real heat sink, the values of t_e and S_e are 1.76 mm and 6.2 mm, respectively.

Table 4 summarises the correlations applied to the heat sink under study. Nu_S is Nusselt number based on fin spacing. It is important to highlight that none of these analytical correlations meet all the geometric characteristics of the heat sink under consideration.

Reference	**Equations**	**Range of parameters**
Jones and Smith [13]	$Nu_S = \left[\left(\frac{Ra_S}{1500}\right)^m + \left(0.081 {Ra_S}^{0.39}\right)^m\right]^{1/m}; m = 2$	0.084≤S/H≤7.69; 0.026≤H/L≤0.19; 0.016≤S/L≤0.20; 200<Ra_S<6·10^5
Rao et al. [10]	$Nu_S = 0.102 {Ra_S}^{0.36}\left(\frac{S}{H}\right)^{0.4}\left(\frac{1+\varepsilon_1}{1+N_R}\right)^{0.1} N^{-0.04}$	0.14≤S/H≤0.83; 0.6≤H/L≤1.4; 0.2≤S/L≤0.5; 2300 < Ra_S <6·10^4; 0.05 < ε_1 < 0.85; 0.3 < N_R < 1
Tari and Mehrtash [14]	$Gr' = \mathrm{Gr}_S (H/L)^{m_1}(S/H)^{m_2}$ $Nu_S = C\,(Gr'Pr)^n$ $m_1 = 0.5; m_2 = 0.38; C = 0.0915; n = 0.436$	0.35 ≤ S/H ≤ 2.94; 0.015 ≤ H/L ≤ 0.1; 0.026≤S/L≤0.059;
Shen et al. [19]	$Nu_S = 2.312 \cdot 10^{-4} Ra_S + 0.377$ [a]	0.12 ≤ S/H ≤ 0.46; H/L = 0.41; 0.05 ≤ S/L ≤ 0.19

Table 4. Summary of correlations for upward facing horizontal heat sinks applied in the present study. [a] Equation obtained from data published in a graph of the article [19].

4.- Numerical model

This section describes the CFD model that was developed to reproduce the real heat sink and the experimental test described in Section 2. ANSYS CFX software was used to perform CFD simulations. Temperatures at the seven monitoring points were used for comparison and model validation.

As $\beta(T-T_0)$ in the present study is less than 1.0, where T_0 is a reference temperature and β is the air thermal expansion coefficient ($1/T_0$), the Boussinesq approximation can be applied. Under this approximation, variations in air density are only dependent on temperature variations, that is:

$$\rho = \rho_0 + \beta(T - T_0) \quad (3)$$

The importance of buoyancy and free convection can be measured by the ratio of the Grashof and Reynolds numbers:

$$\frac{Gr}{Re^2} = \frac{g\beta\Delta T L_C}{\nu^2} \quad (4)$$

Considering fin spacing (S) as the characteristic length (L_C) and using the experimental values of ambient and base plate temperatures, this ratio is about $6 \cdot 10^7$. As this is much greater than one, a strong buoyancy contribution can be expected. Furthermore, Rayleigh numbers less than 10^8 indicates a buoyancy-induced laminar flow, with transition to turbulence occurring over the range $10^8 < Ra < 10^9$. In the present case, Ra_S is 10^3, approximately, showing that the flow is laminar. Then, a steady state 3D laminar air flow was simulated numerically.

Thermal radiation was modelled by Monte Carlo method with Surface to Surface model (S2S) because air was assumed to be optically thin, that is, transparent to thermal radiation [32]. S2S can reduce solution time significantly but no symmetry conditions can be considered, such that heat sink was modelled completely (Fig. 7 a)).

Trying to replicate the experiment, the following boundary conditions were set: inlet heat flux of 7143 Wm^{-2}, equivalent to a heat power of 450W; the heat sink bottom surface was adiabatic. The air, which was assumed as dry air, enters at 26°C through the openings of the enclosure. No slip boundary condition is used for all solid surfaces. The dimensions of the computational domain were 2W x 1.2L x 7H.

An unstructured tetrahedron mesh was used with inflation layers over fin surfaces in order to capture viscous boundary layer as shown in Fig. 7 b). With a target y+ of 1, and characteristic length and air speed of 60 mm and 0.5m/s, respectively, the first nodes were located at about 0.6mm from fin surfaces. Grid independence was checked comparing changes in temperature simulated results at the different monitoring points in the experiment.

Mass, momentum and energy RMS (Root Mean Square) residuals were set to 10^{-4}, while maximum errors in global heat, mass and momentum balances were all smaller than 1.5%. Around 200 to 250 iterations were needed to achieve convergence on average. A high resolution scheme to solve advection terms in discrete equations and double precision were considered for calculations.

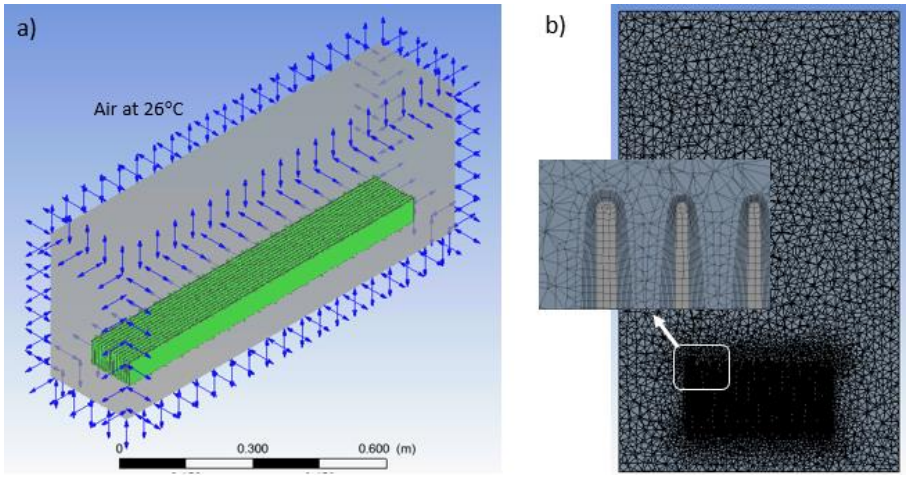

Fig. 7. a) Computational domain. Air at 26°C through enclosure openings. b) Example of unstructured mesh and detail of inflation layers around fin surfaces.

5.- Results and discussion

5.1 Analytical correlations

As it can be seen in Table 5, the results given by the former correlations give base plate temperatures that are about 14 to 23% different from those measured in the experiment.

Reference	T_b(°C)	Relative Error (%)	h (W/m²K)	Nu_S	Ra_S
Experimental Test	128.8	---	2.9	0.5	1330
Jones and Smith [13]	106.3	18	3.3	0.7	1169
Rao et al. [10]	147.1	14	2.5[1]	0.5	1384
Tari and Mehrtash [14]	99.4	23	3.7	0.7	1113
Shen et al. [19]	108.4	16	3.2	0.7	1181

Table 5. Results from the application of different correlations to LCPV heat sink. [1]Average heat transfer coefficient for combined convection and radiation.

Correlation from Rao et al. [10] provides the best results (14%), probably because their correlation is based on a 2D model and then it does not take heat sink length (L) into account. The high length of the heat sink under study can better explain the performance of this correlation since edge effects become less relevant. Furthermore, Tari and Mehrtash correlation achieves the worst result (23%), possibly because S/H ratio in the LCPV heat sink (0.1 approximately), that is known to have significant effect, is quite out of the range for which correlation was set ($0.35 \leq S/H \leq 2.94$). Yet it should be highlighted that the best results (relative errors of 14%) imply deviations of up to 20°C in base plate temperature. Also, discrepancies among correlations varied from 2% to 48%.

5.2 CFD simulations

In order to check mesh independence of numerical results, three different meshes with different mesh densities were used with about 5, 6 and 8 million elements, respectively. Changes of temperature values at monitoring points were smaller than 1°C. All the results presented here are from the medium mesh of 6 million cells.

As it can be seen in Fig. 8, CFD simulations results are very similar to experimental ones, achieving a relative error of about 1% in the estimation of base plate temperature, which is at least ten times smaller than those obtained from correlations. Some of the simulated values are within the experimental error of measured temperatures.

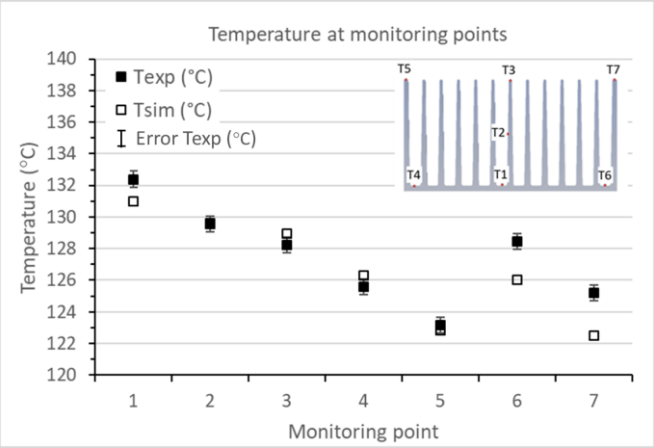

Fig. 8. CFD results vs experimental temperature values at monitoring points.

Fig. 9 shows temperature distribution along the longitudinal and cross sections in the middle of the heat sink and at the rear side of its base. Highest temperature values are found in the central part of the heat sink due to lower air speed and worse convective conditions (Fig. 10 and Fig. 11). Temperature distribution is almost symmetrical as a result of a velocity distribution with higher speed values at the two ends of the heat sink. This dependence also explains that longitudinal variations of temperature (30°C, approximately) are higher (around three times) than variations along transverse sections. Thus, CFD results seem to highlight both cross-sectional and longitudinal effects, which could explain the discrepancies found among correlations.

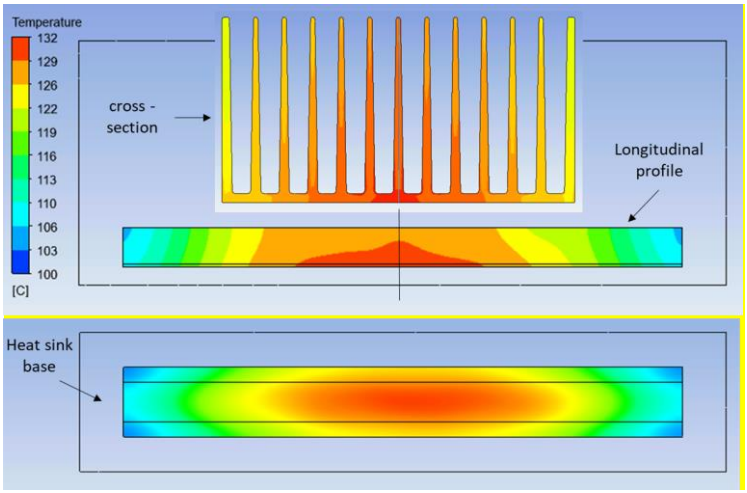

Fig. 9. Up: Temperature contour plots at longitudinal and transverse planes in the central part of the heat sink. Down: Temperature contour plot at the base of the heat sink.

From CFD simulations results, average temperature at the base plate, calculated from temperature estimations at monitoring points 1, 4 and 6, is 127.8°C (relative error of 0.8%), which is significantly different from the predictions made by correlations.

Flow patterns described as single and multiple chimney flows and formerly observed in their experiments by Harahap and McManus [27] can be identified (Fig. 10). According to these authors, the flow is dominated by up and down patterns as the depth of the array becomes larger, typically for L/H ratios between 10 and 20. The present heat sink has an L/H ratio of 15. As it can be seen from Fig. 11, there are also some air stagnation zones around the central part of the heat sink between two main chimney flows, which is a counterproductive effect that worsens heat sink's performance.

CFD simulations can also give both convective and radiative heat fluxes. Thus, average radiative heat flux represents around 10% of total heat flux, which is very similar to the results obtained from the methodologies applied in the present study for radiation calculations ([30], [31]).

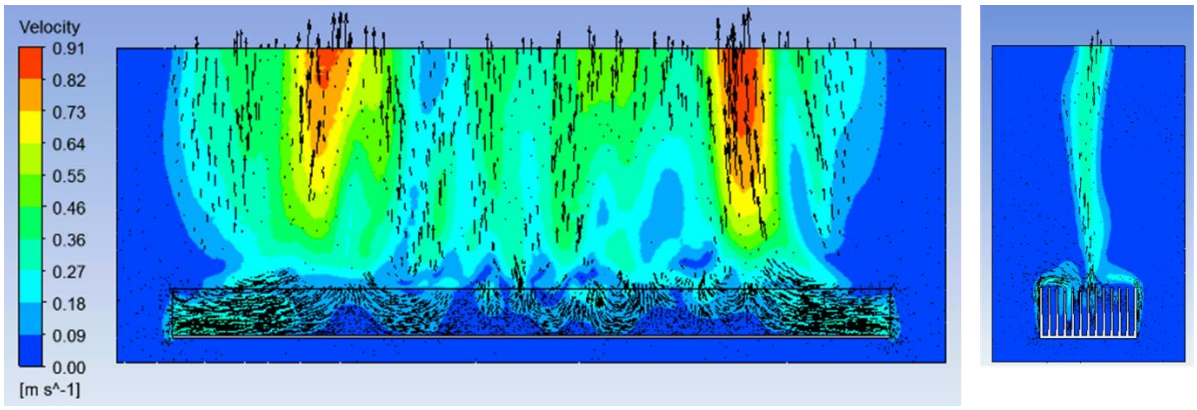

Fig. 10. Velocity contour and vector plots along longitudinal and cross section of the CFD domain.

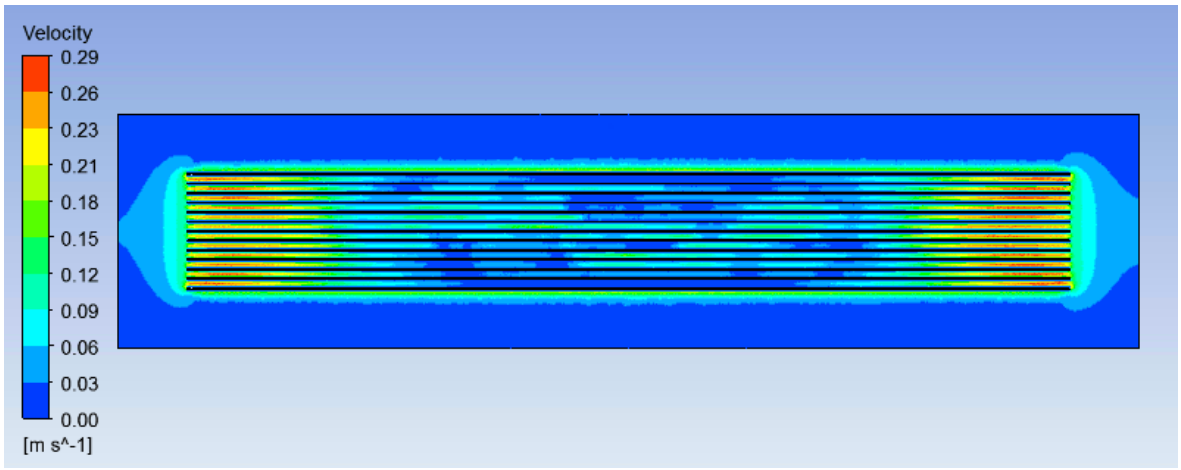

Fig. 11. Top view of velocity contour plot along a longitudinal and horizontal plane at H/2 from the base plate of the heat sink. Stagnation zones in white.

5.3 Performance under different operating conditions

The developed CFD model is used to analyse the heat sink's performance under other operating conditions. Specifically, different inclination angles with respect to the horizontal were considered. Although some authors have undertaken this problem by changing the direction of the gravitational acceleration vector [33], a direct inclination of the geometry is considered in the present study. Five different angles from 0° to 60° (with a fixed increment of 15°) are investigated in this study. The results show that when average base temperature decreases, then inclination angle increases (Fig. 12). This behaviour has also been found by other researchers [28]. Furthermore, air speed increases for higher inclination angles. From the display of velocity and temperature fields at different inclination angles (Fig. 13), it can be seen how the multiple chimney flow pattern and stagnation zones disappear for angles greater than 30° and cooler air enters and flows along the channels between fins. Approximately, 20°C of maximum temperature decrease is found between the different inclination angles. Based on these results, it is expected that the performance of this LCPV heat sink will improve under normal operating conditions.

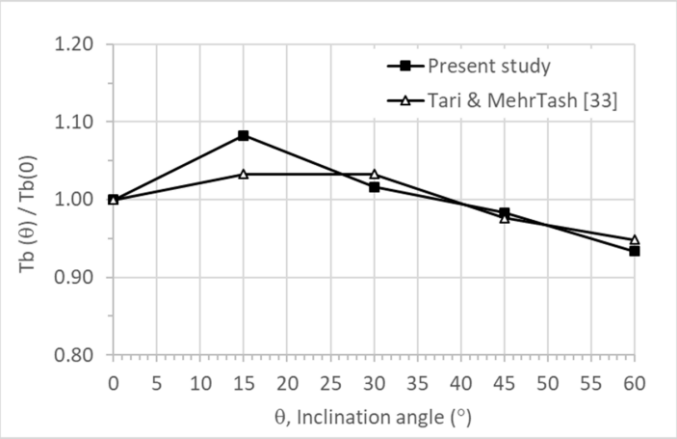

Fig. 12. Variation of base average temperature with inclination angle.

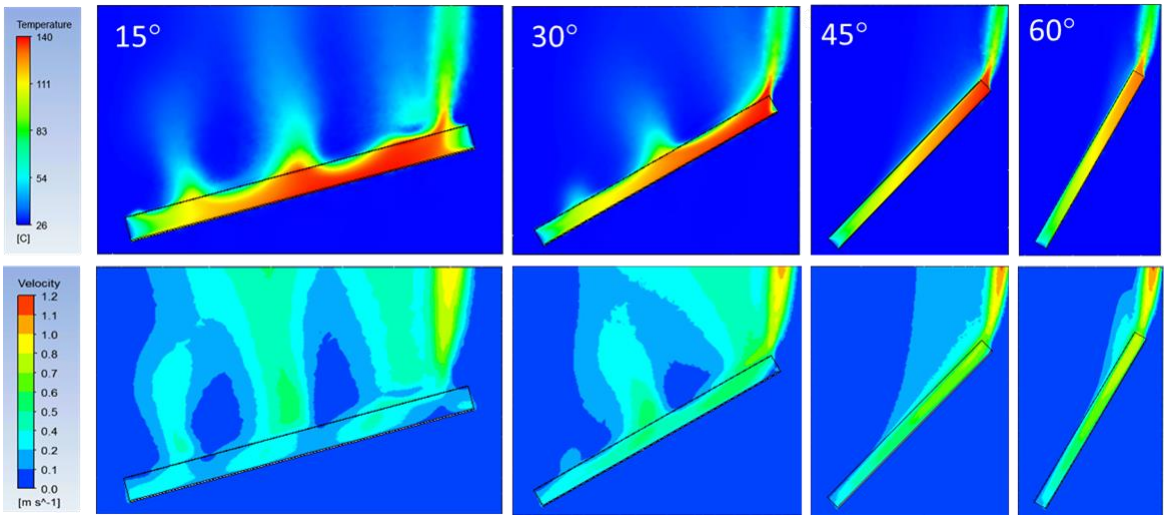

Fig. 13. Temperature and velocity distribution along a longitudinal plane of the air domain for different inclination angles of the heat sink.

6.- Conclusions

The heat sink is a fundamental part of LCPV systems, responsible for decreasing the temperature of the PV receiver. Although there exists a huge number of geometric configurations of heat sinks, one finned heat sink prototype with variable fin thickness and high fin length is considered here. The work is focussed on the analysis, use and selection of different approaches that can be applied to study its thermal performance. In particular, analytical correlations and CFD techniques were used to estimate base plate temperature. An experiment was also developed for comparison of the different approaches.

The most commonly widespread correlations to this kind of heat sinks have been used. These correlations are generally obtained and applicable to heat sinks with constant fin thickness. However, they are frequently used for heat sinks with fins of variable thickness, often assuming an average thickness. Relative errors of up to 23% and deviations of around 20 °C from experimental measurements have been found in the estimation of base plate temperature. Furthermore, discrepancies rose up to 48% among correlations.

Alternatively, CFD numerical simulations were also developed trying to reproduce experimental conditions. Numerical estimations of temperature experimental measurements at monitoring points were very satisfactory, with relative errors of about 1%. Furthermore, patterns of multiple chimney flow conditions and stagnation zones could be identified and explained temperature

distribution. Finally, heat sink performance under different inclination angles was also analysed, showing the disappearance of stagnation areas for inclination angles greater than 30°.

From the results achieved, it can be concluded that more research is necessary to design new configurations of heat sinks in order to get a suitable thermal management of the LCP system.

Acknowledments

This work has been performed with the support of the Spanish government through research projects entitled 'ADVANCED: *Added Value New CPVs Enhanced Developments*' (EXP00064964/ITC-20131056, FEDER-INNTERCONECTA) and "*Desarrollo de sistemas fotovoltaicos de baja concentración con células solares de alta eficiencia y sistemas de seguimiento a un eje*: THESEUS" (RTC-2014-2304-3, RETOS-COLABORACIÓN), both developed in ABENGOA SOLAR NEW TECHNOLOGIES SA. It was also partially carried out during a research stay at the University of Birmingham, with the support of the Programme of Promotion and Encouragement of Research of the University of Cádiz.

References

[1] V.V. Tyagi, Nurul A.A. Rahim, N.A. Rahim, Jeyraj A./L. Selvaraj, Progress in solar PV technology: Research and achievement, Renewable and Sustainable Energy Reviews 20 (2013) 443–461.

[2] M. Steiner, G. Siefer, T. Schmidt, M. Wiesenfarth, F. Dimroth, A. W. Bett, 43% Sunlight to Electricity Conversion Efficiency Using CPV, IEEE Journal of Photovoltaics 6 (4) (2016) 1020–1024.

[3] F. Famoso, R. Lanzafame, S. Maenza, P.F. Scandura, Performance comparison between Low Concentration Photovoltaic and fixed angle PV systems, Energy Procedia 81 (2015) 516 – 525.

[4] H. Chen, J. Ji, Y. Wang, W. Sun, G. Pei, Z. Yu, Thermal analysis of a high concentration photovoltaic/thermal system, Solar Energy 107 (2014) 372–379.

[5] R.J. Linderman, Z.S. Judkins, M. Shoecraft, M.J. Dawson, Thermal Performance of the SunPower Alpha-2 PV Concentrator, IEEE Journal of Photovoltaics 2(2) (2012) 196-201.

[6] A. Shukla, K. Kant, A. Sharma, P.H. Biwole, Cooling methodologies of photovoltaic module for enhancing electrical efficiency: A review, Solar Energy Materials and Solar Cells 160 (2017) 275–286.

[7] J. Siecker, K. Kusakana, B.P. Numbi, A review of solar photovoltaic systems cooling technologies, Renewable and Sustainable Energy Reviews 79 (2017) 192–203.

[8] J.R. Culham, M.M. Yovanovich, S. Lee, Thermal modelling of isothermal cuboids and rectangular heat sinks cooled by natural convection, IEEE Transactions on Components, Packaging and Manufacturing Technology, Part A 18(3) (1995) 559-566.

[9] S.K. Natarajan, T.K. Mallick, M. Katz, S. Weingaertner, Numerical investigations of solar cell temperature for photovoltaic concentrator system with and without passive cooling arrangements, International Journal of Thermal Sciences 50 (2011) 2514–2521.

[10] V.D. Rao, S.V. Naidu, B.G. Rao, K.V. Sharma, Heat transfer from a horizontal fin array by natural convection and radiation—A conjugate analysis, International Journal of Heat and Mass Transfer 49 (2006) 3379–3391

[11] V. Rammohan Rao and S.P. Venkateshan, Experimental study of free convection and radiation in horizontal fin arrays, International Journal of Heat and Mass Transfer 39 (1996) 779-789.

[12] M. Corcione, Heat transfer correlations for free convection from upward-facing horizontal rectangular surfaces. Proceedings of WSEAS Transactions on Heat and Mass Transfer, Vol. 2, Issue 3 (2007) 48-60.

[13] C.D. Jones and L.F. Smith, Optimum arrangement of rectangular fins on horizontal surfaces for free-convection heat transfer, Journal of Heat Transfer 92 (1) (1970) 6–10.

[14] I. Tari and M. Mehrtash, Natural convection heat transfer from horizontal and slightly inclined plate-fin heat sinks, Applied Thermal Engineering 61 (2013) 728-736.

[15] W. Elenbaas, Heat dissipation of parallel plates by free convection, Physica IX, N°1 (1942) 1-28.

[16] W.M. Rohsenov, J.P. Hartnett, Y.I. Cho. Handbook of heat transfer. McGraw-Hill 1998.

[17] A. Bar-Cohen, M. Iyengar, A.D. Kraus, Design of optimum plate-fin natural convective heat sinks, Transactions of the ASME 125 (2003) 208-216.

[18] K.H. Do, T.H. Kim, Y-S. Han, B-I. Choi, M-B. Kim, General correlation of a natural convective heat sink with plate-fins for high concentrating photovoltaic module cooling, Solar Energy 86 (2012) 2725–2734.

[19] Q. Shen, D. Sun, Y. Xu, T. Jin, X. Zhao, Orientation effects on natural convection heat dissipation of rectangular fin heat sinks mounted on LEDs, International Journal of Heat and Mass Transfer 75 (2014) 462–469.

[20] M. Lee, H.J. Kim, D-K. Kim, Nusselt number correlation for natural convection from vertical cylinders with triangular fins, Applied Thermal Engineering 93 (2016) 1238–1247.

[21] M. Dogan, M. Sivrioglu, O. Yilmaz, Numerical analysis of natural convection and radiation heat transfer from various shaped thin fin-arrays placed on a horizontal plate - a conjugate analysis, Energy Conversion and Management 77 (2014) 78–88.

[22] X. Meng, J. Zhu, X. Wei, Y. Yan, Natural convection heat transfer of a straight-fin heat sink, International Journal of Heat and Mass Transfer 123 (2018) 561–568.

[23] S. Feng, M. Shi, H. Yan, S. Sun, F. Li, T.J. Lu, Natural convection in a cross-fin heat sink, Applied Thermal Engineering 132 (2018) 30–37.

[24] H. Mousavi, A. A.R. Darzic, M. Farhadib, M. Omidi. A novel heat sink design with interrupted, staggered and capped fins, International Journal of Thermal Sciences 127 (2018) 312–320.
[25] V.A.F. Costa and A.M.G. Lopes, Improved radial heat sink for led lamp cooling, Applied Thermal Engineering 70 (2014) 131-138.
[26] N.S. Effendi and K.J. Kim, Orientation effects on natural convective performance of hybrid fin heat sinks, Applied Thermal Engineering 123 (2017) 527–536.
[27] F. Harahap and H.N. McManus, Natural convection heat transfer from horizontal rectangular fin arrays, Journal of Heat Transfer (1967) 32–38.
[28] X. Luo, W. Xiong, T. Cheng, S. Liu, Design and optimization of horizontally-located plate fin heat sink for high power LED street lamps, Electronic Components and Technology Conference, San Diego, CA, USA, IEEE (2009) 854-859.
[29] M. Dogan and D. Dogan, Experimental investigation of natural convection heat transfer from fin arrays for different tip-to-base fin spacing ratios, Journal of Thermal Science and Technology 37 (1) (2017) 147-157.
[30] Y. Shabany, Radiation Heat Transfer from Plate-Fin Heat Sinks, Twenty-fourth Annual IEEE Semiconductor Thermal Measurement and Management Symposium. 16-20 March (2008). San Jose, CA, USA.
[31] S.N. Rea and S.E. West, Thermal radiation from finned heat sinks, IEEE Transactions on Parts, Hybrids, and Packaging 12 (2) (1976) 115–117.
[32] Ansys Fluent 12.0, Theory Guide, 2009.
[33] I. Tari and M. Mehrtash, Natural convection heat transfer from inclined plate-fin heat sinks, International Journal of Heat and Mass Transfer 56 (2013) 574–593.